Modes of Interannual and Interdecadal Variability of Pacific SST

XUEBIN ZHANG

Climate Research Branch, Atmospheric Environment Service, Downsview, Ontario, Canada

JIAN SHENG

Canadian Centre for Climate Modelling and Analysis, Atmospheric Environment Service, Victoria, British Columbia, Canada

AMIR SHABBAR

Climate Research Branch, Atmospheric Environment Service, Downsview, Ontario, Canada

(Manuscript received 16 June 1997, in final form 31 October 1997)

ABSTRACT

The multichannel singular spectrum analysis has been used to characterize the spatio–temporal structures of interdecadal and interannual variability of SST over the Pacific Ocean from 20°S to 58°N. Using the Comprehensive Ocean–Atmosphere Data Set from 1950 to 1993, three modes with distinctive spatio-temporal structures were found. They are an interdecadal mode, a quasi-quadrennial (QQ) oscillation with a period of 51 months, and a quasi-biennial (QB) oscillation with a period of 26 months. The interdecadal mode is a standing mode with opposite signs of SST anomalies in the North Pacific and in the tropical Pacific. The amplitude of this mode is larger in the central North Pacific than in the tropical Pacific. This mode contributes 11.4% to the total variance. It is associated with cooling in the central North Pacific and warming in the equatorial Pacific since around 1976–77. The QQ oscillation exhibits propagation of SST anomalies northeastward from the Philippine Sea and then eastward along 40°N, but behaves more like a standing wave over the tropical Pacific. It explains nearly 20% of the total variance. The QB oscillation is localized in the Tropics and is characterized by the westward propagation of SST anomalies near the equator. This mode accounts for 7.4% of the total variance. Since the interdecadal mode is apparently independent of QB and QQ oscillations, it may play an important role in configuring the state of the tropical SST anomalies, which in turn affects the strength of the El Niño–Southern Oscillation phenomenon. It seems likely that the higher phase of the interdecadal mode since 1976–77 has raised the background SST state, on which the superposition of the QQ and QB oscillations produced the strongest warm event on record in 1982–83, as well as more frequent warm events since 1976.

1. Introduction

Recently, there has been considerable interest in describing climate variability over the Pacific basin on decadal and longer timescales. Many of these investigations are motivated by the desire to understand the role of natural variability in explaining recent significant changes in the Pacific SSTs, for example, cooling in the North Pacific and warming in the tropical regions since about 1976–77 (Trenberth and Hoar 1996). It has been observed that El Niño events have been more frequent and La Niña events less frequent since the late 1970s (e.g., Trenberth 1990; Trenberth and Hurrell 1994; Trenberth and Hoar 1996). Moreover, the characteristics of the onset of El Niño since the late 1970s have also changed (Wang 1995). On the other hand, changes in the El Niño–Southern Oscillation (ENSO) have also been linked to the decadal climate variability throughout the Pacific basin (e.g., Trenberth and Hurrell 1994). A better understanding of the SST variation at different timescales in various regions of the basin is therefore needed.

By applying principal component analysis (PCA) on the 7-yr running mean of the tropical Pacific SST anomalies (SSTA), Wang (1995) attributed these changes to a concurrent shift in the background state of the mean SST since 1976–77. Based on a multichannel singular spectrum analysis (MSSA) on detrended SSTA in the equatorial Pacific, Jiang et al. (1995) found two ENSO-related interannual modes, the quasi-quadrennial (QQ) mode with a period of 52 months and the quasi-biennial (QB) mode with periods from 24 to 28 months. They showed that the differences between two ENSO-related interannual modes in the tropical Pacific SSTs depend

Corresponding author address: X. Zhang, Climate Research Branch, Atmospheric Environment Service, 4905 Dufferin St., Downsview, ON, M3H 5T4, Canada.
E-mail: Xuebin.Zhang@ec.gc.ca

not only on frequency, but also on the way SST anomalies propagate. The QQ mode represents a standing oscillation of the SSTA in the eastern equatorial Pacific, whereas the QB mode exhibits slight westward propagation of the SSTA from the eastern to central Pacific. The secular change in the tropical SST since about 1976–77 as identified by Wang (1995) was not obvious in Jiang et al.'s (1995) findings, due to their detrending of the SST time series. Connections between the SST variations in the Tropics and in the North Pacific at both interannual and interdecadal timescales are evident. Reynolds and Rasmusson (1983) composited six El Niño events between 1949 and 1980 and found that during the Northern Hemisphere fall and winter—the transition and mature phase of El Niño—an east–west-oriented elliptical cold pool develops in the central Pacific and warm water extends along most of the west coast of North America. Such a connection was also successfully simulated by ocean models (e.g., Alexander 1990) and confirmed by other observational studies (e.g., Lau 1997). In an analysis of the Pacific (north of 20°S) SSTA, Zhang et al. (1997) found that the spatial signature of SST associated with the ''ENSO cycle-related'' variability on the interannual timescale and that associated with the interdecadal variability are of a spatial scale of the entire basin, and that there are only subtle differences between the spatial signatures corresponding to different timescales. There may also exist a North Pacific mode that is linearly independent of the ENSO-related mode, as suggested by Deser and Blackmon (1995).

Although the interannual and interdecadal variabilities have quite different timescales, PCA studies indicate their spatial patterns are rather similar. Tanimoto et al. (1993) investigated temporal evolution and spectral structure of SSTA in the North Pacific during 1950–86 on three characteristic timescales: shorter than 24 months, 24–60 months, and longer than 60 months. They found that leading EOF for shorter than 24 months timescale is somewhat similar to that for a timescale longer than 60 months. Zhang et al. (1997) showed that the spatial patterns of the interannual and interdecadal variabilities of Pacific SST are both characterized by SST anomalies along the equator and North Pacific anomalies of opposite sign. In the Pacific, the only difference shown by PCA is that the interannual mode has a narrower and sharper temperature tongue in the Tropics and weaker extratropical anomalies. The question remains whether such similarity in the spatial patterns associated with the interannual and interdecadal variabilities reflects the nature of the frequency dependence of the system itself. It is possible that the interannual and interdecadal variabilities are separate modes with distinctive periods, spatial patterns, and characteristic propagation of SST anomalies, but the PCA of the high- and low-pass-filtered data is unable to distinguish them.

It appears that there is still a need to characterize Pacific SST variability, at both interdecadal and interannual timescales, in the context of both spatial and temporal evolutions of SSTA. The analysis may provide us with a better understanding of the relationship between the tropical and the North Pacific SST anomalies and the possible role of slower (interdecadal) and ENSO-related modes in determining the SST variability in the Pacific.

In this study, MSSA has been applied to investigate the spatial and temporal structures of Pacific SST variability at both interdecadal and interannual timescales, so that the differences between the ENSO-related modes and the slower interdecadal mode can be better quantified. In particular, we will address the question of the separability of the ENSO-related modes and the interdecadal mode. The use of MSSA technique allows us to simultaneously identify oscillations with widely different timescales without commonly used prefiltering of data.

The data and main analysis tools are described in section 2. The modes of interdecadal and interannual variability and their temporal structures are compared in sections 3 and 4, respectively. Concluding remarks follow in section 5.

2. Data and strategy

The monthly mean SST over the Pacific Ocean between 20°S and 58°N, derived from the Comprehensive Ocean–Atmosphere Data Set (Woodruff et al. 1987) for the period from January 1950 to December 1993, are used in this study. To identify interdecadal and interannual variability and to make a more reliable estimation of the monthly means, the original 2° lat × 2° long data are first transferred onto 4° lat × 8° long by averaging all available data in the 4° × 8° grid box, greatly reducing data gaps. No missing values were found in the 4° × 8° grids north of 20°N. The missing data in the Tropics were interpolated as follows: if data for both neighboring grid points (either in latitude or in longitude) were available, linear interpolation from adjacent points was used; otherwise, the values for adjacent months were averaged as the estimate if data for both preceding and following months at the same grid point were available; a bivariate interpolation in space was used for filling the few remaining gaps. To isolate the modes of interdecadal and interannual variability, the seasonal cycle was removed by subtracting the long-term mean of SST in each calendar month at each grid box.

PCA is frequently used to identify the dominant coherent spatial structures and their strengths in time of an L-variate time series. The spatial patterns are represented by the (spatial) empirical orthogonal functions (S-EOFs) or the eigenvectors of the covariance matrix of the fields. The strengths of the EOFs are represented by the corresponding principal components (S-PCs). To take the persistence of climate variables into account, this approach may be generalized by considering time

as another variate: at each time t, the fields are considered simultaneously at time t, $t + 1$, $t + 2$, . . . , $t + M - 1$, so that the temporal evolution during M steps becomes part of the mode structure. That is, PCA is performed on an augmented dataset, which has $M \times L$ ''variables'' consisting of M lagged (with lags from 0 to $M - 1$) copies of the original data. The main patterns identified are coherent in space and time: they consist of a spatial pattern for each of the M time slices and are called spatio–temporal EOFs (ST-EOFs). The strengths of those ST-EOFs are represented by corresponding principal components (PCs), which are termed spatio–temporal PCs (ST-PCs). This generalization of PCA is called space–time PCA or MSSA. Here M is called window length. In MSSA, a quasi-oscillating structure is represented by a pair of ST-EOFs and ST-PCs explaining a similar amount of variance and having the same dominant frequency and relative phase difference of one-quarter of a period. Detailed descriptions and properties of MSSA can be found in Plaut and Vautard (1994). The ability to concurrently distinguish between different dominant spatio-temporal modes of variability (Wang et al. 1996; Plaut and Vautard 1994) makes MSSA ideally suited for the current study.

The power spectra of ST-PCs were computed using the maximum entropy method based on the algorithm of Barrodale and Erickson (1980). To identify oscillatory pairs, we have used the same criteria as those employed by Wang et al. (1996). A pair of eigenmodes is said to be an oscillatory pair if 1) the frequencies f_k and f_{k+1}, respectively, corresponding to the maximum spectral values of ST-PC$_k$ and ST-PC$_{k+1}$ satisfy $2M|f_k - f_{k+1}| < 0.75$ (Vautard et al. 1992); 2) the two extrema on either side of 0, of the lagged correlation between ST-PC$_k$ and ST-PC$_{k+1}$ are larger than 0.5; 3) there exists at least one complete cycle of the oscillation in the window length M for the pair ST-EOF$_k$ and ST-EOF$_{k+1}$.

Vautard et al. (1992) show that if the dataset is sufficiently long, and if M is less than one-third of the sample size, the SSA can usually isolate oscillatory behavior with periods in the range of (M/5, M). Since we used a window size of 61 months, we should be able to distinguish periods of 1–5 yr. Lower frequencies can still be identified, though they would not form separate pairs of eigenmodes. To obtain the ST-EOFs—that is, to solve the eigen problem for the lag-cross-covariance matrix of dimension $(L \times M) \times (L \times M)$—in practice, the size of the matrix has to be not too large (i.e., the matrix should be generally smaller than available computer memory), thus the number of variables L for the MSSA has to be small enough. We first performed PCA on the SSTA to compress information, and retained only the first 10 PCs, which explain 47.7% of the total variance for the subsequent MSSA. In fact, MSSA is not sensitive to the truncation point of this PCA; retaining 6 PCs (explaining 37.6% of the total variance) or 15 PCs (explaining 54.8% of the total variance) does not significantly alter the results to be presented in the following two sections. When performing PCA, we computed the covariance matrices with and without weighting SSTA at each grid point by the square root of the cosine of latitude and found that it made very little difference. The results of MSSA performed on the first 10 PCs obtained from weighted and unweighted SSTA proved to be essentially the same. Wallace et al. (1992) also pointed out that unweighting SSTA has little effect on describing covariance structures of the Pacific SST. For simplicity, the following results are based on the application of MSSA on the PCs of SSTA without weighting at individual grid.

A formal assessment of statistical significance of identified modes is difficult. Nevertheless, a certain level of confidence can still be established by examining various aspects of identified modes.

1) According to North et al. (1982), a ''typical error'' of the estimated kth eigenvalue λ_k in an EOF analysis is given by

$$\Delta\lambda_k \simeq \lambda_k\sqrt{2/n},$$

where n is the effective sample size. We use N/N_o as the estimate of n, with N being the sample size and N_o being the ''decorrelation time.'' The average of n's for all variables was used as the representative equivalent sample size. If two eigenvalues, $\lambda_k > \lambda_{k+1}$, satisfy

$$\lambda_k < \lambda_{k+1} + \Delta\lambda_k + \Delta\lambda_{k+1},$$

then corresponding patterns (eigenvectors) EOF$_k$ and EOF$_{k+1}$ are a random mixture of the true patterns—that is, the two patterns are ''mixed up.'' In our particular application, the errors of the estimated eigenvalues are used to examine the closeness of two consecutive eigenvalues λ_k and λ_{k+1} and hence the mixing of patterns. In addition, if in the eigenvalue spectrum an oscillatory pair is well separated from its neighbor eigenvalues, it may be concluded that the spatio-temporal evolution of this oscillation is not likely to be contaminated by others. Therefore, one can be fairly confident that the spatio-temporal structures revealed by that oscillatory pair do reflect real structures.

2) The reproducibility of ST-EOFs was also examined. The 1950–93 SSTA record was split into two equal parts—that is, from 1950 to 1971 and from 1972 to 1993 (hereafter referred to as subsets 1 and 2); PCA and MSSA were performed on the two parts separately, resulting in two sets of ST-EOFs (ST-PCs); the subset 1 (subset 2) was then projected onto the ST-EOFs of subset 2 (subset 1), resulting in two sets of ''projected'' ST-PCs (PST-PCs); the ST-PCs and PST-PCs of the same subset were then compared.

3) It is important to distinguish a potential climate signal from red noise, since temporal autocorrelation may lead to ST-PCs that are entirely due to noise masquerading as high-variance low-frequency oscillations (Allen and Smith 1996). We adapted the Monte-Carlo SSA of Allen and Smith (1996) to determine if the ST-EOFs are significantly different from what one could

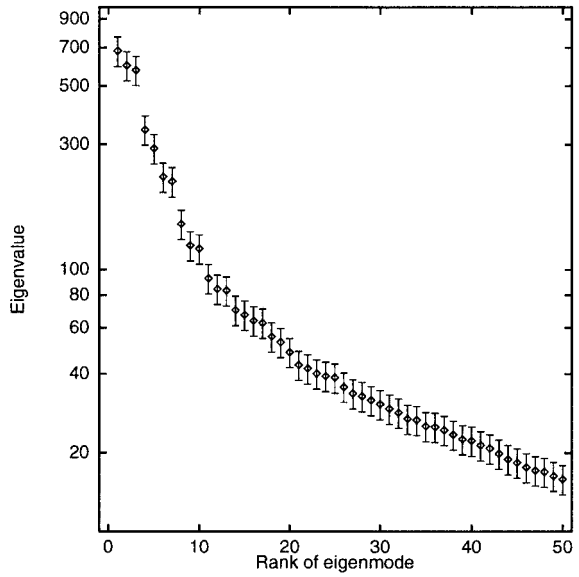

FIG. 1. The first 50 largest eigenvalues along with their sampling errors calculated according to North et al. (1982).

obtain from pure red noise. A red noise model, which consists of 10 independent AR(1) processes, each with the same variance and first-order autocorrelation as those of the first 10 PCs, is used to generate 100 segments of noise data with the same sample size as the observation. The ''eigenvalue'' (or variance) of the noise in the direction of phase space defined by an ST-EOF was obtained by projecting the noise onto that ST-EOF. We computed the ratio of an eigenvalue of MSSA to the 97.5th largest ones of its counterparts in the 100 segments of the noise. If a ratio is greater than 1, the corresponding ST-EOF is then considered to be significantly different from red noise at 2.5% level. If the SST anomalies are significantly different from red noise, the parameters of AR(1) processes directly estimated from the first 10 PCs of SSTA could be biased. Unbiased parameters may be obtained by taking the known (identified) signals into account (Allen and Smith 1996).

3. Modes of interannual and interdecadal variability

The 50 largest eigenvalues of ST-EOF along with their sampling errors, computed according to North et al. (1982), are plotted in Fig. 1. There are three pairs of nearly equal eigenvalues, namely, eigenvalues 2 and 3, 6 and 7, and 9 and 10. Among them, the eigenvalues 6 and 7 are best separated from their neighbors. Eigenvalues ranked after 10 are generally not separable. This may suggest a limit beyond which MSSA cannot identify useful signals in this particular dataset.

The cross correlations between ST-PCs and PST-PCs for both subsets were computed. Only the first seven leading ST-PCs show high correlations, which are displayed in Table 1. For both subsets, ST-PCs 1–4 are, respectively, highly correlated with PST-PCs 1–4. For subset 1, the ST-PCs 6–7 and PST-PCs 5–6 are highly correlated; for subset 2, ST-PCs 5–6 and PST-PCs 6–7 are highly correlated. These high correlations imply the close correspondence between the ST-EOFs 1–4 and 6–7 of subset 1 and ST-EOFs 1–6 of subset 2, respectively. The ST-PCs 1–6 of subset 2 and ST-PCs 1–4 and 6–7 of subset 1 are related with ST-PCs 1–4 and 6–7 of the entire dataset at even higher correlations (not shown), suggesting that the ST-EOFs 1–4 and 6–7 of the complete dataset correspond to ST-EOFs 1–4 and 6–7 of subset 1 or ST-EOFs 1–6 of subset 2, respectively, and are quite stable.

The ratios of the first 50 MSSA eigenvalues of SSTA to the 97.5th largest ones of their counterparts in the 100 segments of red noise are displayed in Fig. 2. The Monte Carlo test appears to suggest that ST-EOFs 2–12, 19–20, 22–24, 30, 32–35, 37, 42, and 47 are individually significant at 2.5%. When ST-EOFs 2–3 and 6–7 are considered as ENSO signals (see following discussion), ST-EOFs 1 and 18 are also significant (Fig. 3).

Based on the aforementioned three different tests, we may conclude that there exist six stable ST-EOFs (ST-EOFs 1–4 and 6–7), which may represent identifiable signal from SSTA by the MSSA. We will focus on these ST-EOFs in the remainder of this paper.

a. Interannual modes

The ST-PCs 2–3 and 6–7 also satisfy the oscillatory pair selection criteria. These two oscillatory ST-PC pairs have peaks in their power spectra at the periods of 51 and 26 months, respectively, indicating that they tend to oscillate at those periods. Plaut and Vautard (1994) pointed out that the total power spectrum of the input

TABLE 1a. Cross correlations between leading ST-PCs calculated from SSTA for 1950–71 and projections (PST-PCs) of SSTA for that period on the relevant ST-EOFs computed from SSTA for 1972–93.

	ST-PC1	ST-PC2	ST-PC3	ST-PC4	ST-PC5	ST-PC6	ST-PC7
PST-PC1	−0.22	0.11	**0.97**	−0.37	0.01	−0.08	−0.64
PST-PC2	0.44	**0.94**	−0.05	−0.04	−0.11	0.12	0.16
PST-PC3	**0.77**	−0.23	−0.15	−0.16	−0.13	−0.10	−0.16
PST-PC4	0.14	−0.20	0.14	**0.88**	−0.07	−0.10	0.35
PST-PC5	−0.29	−0.01	−0.14	0.21	0.55	−0.11	0.31
PST-PC6	0.14	−0.05	0.12	0.05	**0.72**	0.17	−0.20
PST-PC7	0.10	−0.09	0.04	−0.03	0.21	**−0.87**	−0.35

TABLE 1b. Cross correlations between leading ST-PCs calculated from SSTA for 1972–93 and projections (PST-PCs) of SSTA for that period on the relevant ST-EOFs computed from SSTA for 1950–71.

	PST-PC1	PST-PC2	PST-PC3	PST-PC4	PST-PC5	PST-PC6	PST-PC7
ST-PC1	0.12	−0.05	**0.97**	0.03	0.08	0.07	−0.39
ST-PC2	0.33	**0.95**	−0.04	0.15	−0.02	0.15	−0.27
ST-PC3	**0.85**	−0.32	0.10	−0.43	−0.27	−0.08	−0.14
ST-PC4	0.08	−0.09	0.51	**0.81**	−0.22	−0.11	0.21
ST-PC5	−0.56	0.29	−0.21	0.32	0.66	−0.21	0.19
ST-PC6	0.42	0.09	0.27	−0.09	**0.76**	0.06	0.01
ST-PC7	0.12	−0.01	−0.09	0.09	0.18	**−0.95**	−0.08

data for MSSA is the sum of power spectra of all ST-PCs. Therefore, in the frequency domain, the variance contribution of a ST-PC is the fraction of the power spectrum of that ST-PC in the total power spectrum of the data. The variance contributions of each oscillatory pair, which were obtained by summing the power spectra of the two ST-PCs of the pair and then being divided by the total power spectrum of the data, are plotted in Fig. 4. About 75.0% (57%) of the variance at the period of 51 (about 26) months is contributed by the ST-PCs 2–3 (ST-PCs 6–7). The ST-PC 4 has a peak in its power spectrum at 33 months. However, this ST-PC does not form a stable oscillatory pair with its neighboring ST-PCs and we are not quite sure what this really means and hence will not discuss it further.

The first oscillatory pair (ST-PCs 2–3), representing a 51-month oscillation, explains 19.7% of the total variance. This oscillation consists of phase alternations of intense anomalies over the North Pacific matched by anomalies of opposite sign over the Tropics extending to the west coast of North America. In the Tropics, the SST anomalies appear as standing waves, while in the extratropics the anomalies propagate northeastward from the Philippine Sea and then eastward in the central North Pacific. A half-cycle of this oscillation is illustrated in Fig. 5 with either 3- or 4-month intervals between maps. We normalized ST-PCs and use their standard deviations to multiply the corresponding ST-EOFs, thus the ST-EOFs have a unit in a degree of Celsius. Starting from a full-blown El Niño phase in Fig. 5a, the warm tongue of SST in the Tropics weakens quickly (Figs. 5a–c) and eventually reverses its sign (Fig. 5d). The negative anomalies then strengthen (Figs. 5e–g) and finally weaken after they peak in Fig. 5g. In the second half of the cycle, which may be viewed from Figs. 5a–h but with a reversed sign, the tropical SST anomalies complete the 51-month period as a standing oscillation. On the other hand, the midlatitude anomalies appear as a traveling oscillation. A weak positive anomaly center moves from the Philippine Sea northeastward to (30°N, 170°W) in about 11-months (Figs. 5a–d), where it extends northwestward (Fig. 5e) and then amplifies while moving eastward (Figs. 5f–h). It reaches the highest

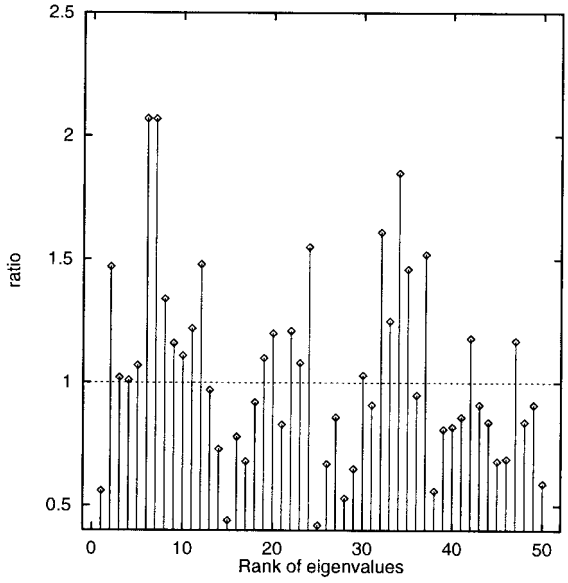

FIG. 2. The ratios of MSSA eigenvalues of SST data and the 97.5% largest eigenvalue expected in the directions defined by the corresponding ST-EOFs in a segment of AR(1) noise. A value equal to or larger than 1.0 implies that the corresponding ST-EOF (ST-PC) is significantly different from red noise at 2.5%.

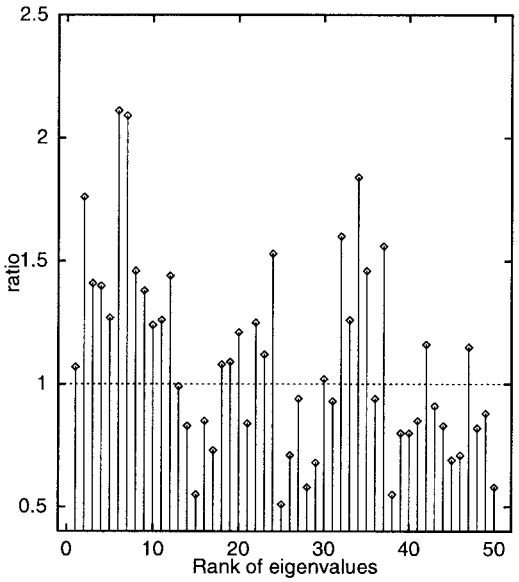

FIG. 3. The same as Fig. 2, except the ST-EOFs/PCs 2, 3, 6, and 7 are considered as ''signal''.

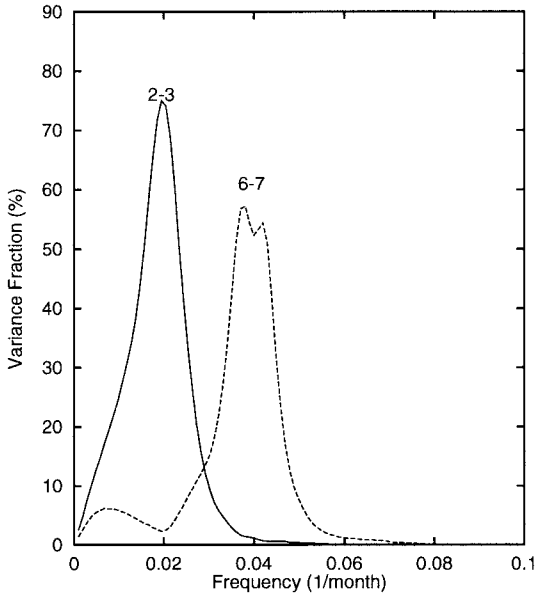

FIG. 4. Variance fractions (in percentage) of the identified pairs of ST-PCs of the Pacific SST, derived by MSSA with a window length of 61 months.

positive amplitude in Fig. 5h. In the second half of the cycle, the positive anomaly center (shown as the negative center in Figs. 5a–e), weakens and moves farther eastward. When it reaches the west coast of North America, it merges into the warm pool of SST along the coast (the reverse of Figs. 5f–h). It is apparent that the strongest oscillations occur in the Tropics and that the North Pacific SST anomalies reach their maximum 3–4 months later than the tropical anomalies do (with opposite sign). We should also mention that, although the SST anomalies in the region between Tropics and the central North Pacific are relatively weak compared with their counterparts in the tropical Pacific or the central North Pacific, they may still be important—that is, since the total variance of SST in that region is typically one-third to one-half of the variance in the Tropics or in the central North Pacific (not shown). It is also noted that, during the journey all the way across the North Pacific, the maximum amplitude of the SST anomalies is reached near the date line. The ENSO mode, or the first EOF of the winter SST anomalies over the Pacific as identified by Deser and Blackmon (1995), can be identified as one of the phases of this oscillation (e.g., Figs. 5b and 5h). In terms of the period and wave propagation over the Tropics, this oscillation is similar to the QQ mode identified by Jiang et al. (1995) in their detrended tropical Pacific SST dataset. We therefore also call this oscillation the QQ mode.

The second oscillatory pair (ST-PCs 6–7) identified by MSSA has a 26-month period, explaining 7.4% of the total variance. The most striking feature of this mode is the westward propagation of SST anomalies over the tropical Pacific. Figure 6 shows eight phases of this oscillation in almost one complete cycle. It can be observed that the mature phase of La Niña (Fig. 6a) in the Tropics is matched by positive anomalies over the central North Pacific and negative anomalies off the coast of North America. After this phase of La Niña, the anomalies weaken basinwide and the positive anomalies over the central North Pacific shift east-southeastward (Fig. 6b). Six months later (Fig. 6c), the weakened negative center in the Tropics has moved to about 160°W, whereas positive anomalies appear over the east tropical Pacific and subsequently propagate westward. It takes about 4–5 months for the positive anomalies to dominate the entire tropical area (Fig. 6d) and another 2–3 months to become strongest in the cycle, which could be classified as the mature phase of El Niño (Fig. 6e). Afterward, the anomalies weaken basin wide again, and an area with negative anomalies emerges in the eastern tropical Pacific in about 3–4 months (Fig. 6f). The negative anomalies propagate westward and then extend into the whole tropical area in 5 months (Fig. 6h), and another La Niña–El Niño cycle begins. It was noted that the amplitudes of the centers of anomalies weaken when the centers move westward. The propagation of SST anomalies in the North Pacific is less systematic, and the 26-month period cannot be identified if the MSSA is applied to North Pacific SST alone, suggesting that the 26-month oscillation is localized in the Tropics. We will come back to this point later. Similar to the QQ mode, the strongest anomalies also appear in the Tropics. In the tropical Pacific, this oscillatory pair behaves similarly to the QB mode of Jiang et al. (1995), both in the period and the way anomalies propagate over the region. We name this oscillation QB mode.

The interannual mode of Zhang et al. (1997), obtained by regressing global SSTs on the ''cold tongue'' region in the tropical Pacific, is very similar to the phases of our QQ and QB modes that correspond to the strongest SSTAs in the Tropics (i.e., the mature phase La Niña or El Niño). This is not surprising since it is the strongest SSTA that make the greatest contribution to the variance and hence the fitting of the regression. The MSSA technique indicates, however, that there are two modes of interannual variability, with different frequencies and distinctive characteristics of propagation of the SST anomalies.

b. Interdecadal mode

The average of the ST-EOF1 for the lags from 0 to 60 months is plotted in Fig. 7. ST-EOF1 is a standing mode, with a negative sign over the Tropics and the west coast of North America and a positive sign over the remaining areas. At the same grid point, there is no change in the sign of anomalies among the maps of the ST-EOF at time lags from 0 to 60 months; the differences of the values among maps are also small, for example, ST-EOF1 at the positive (negative) center var-

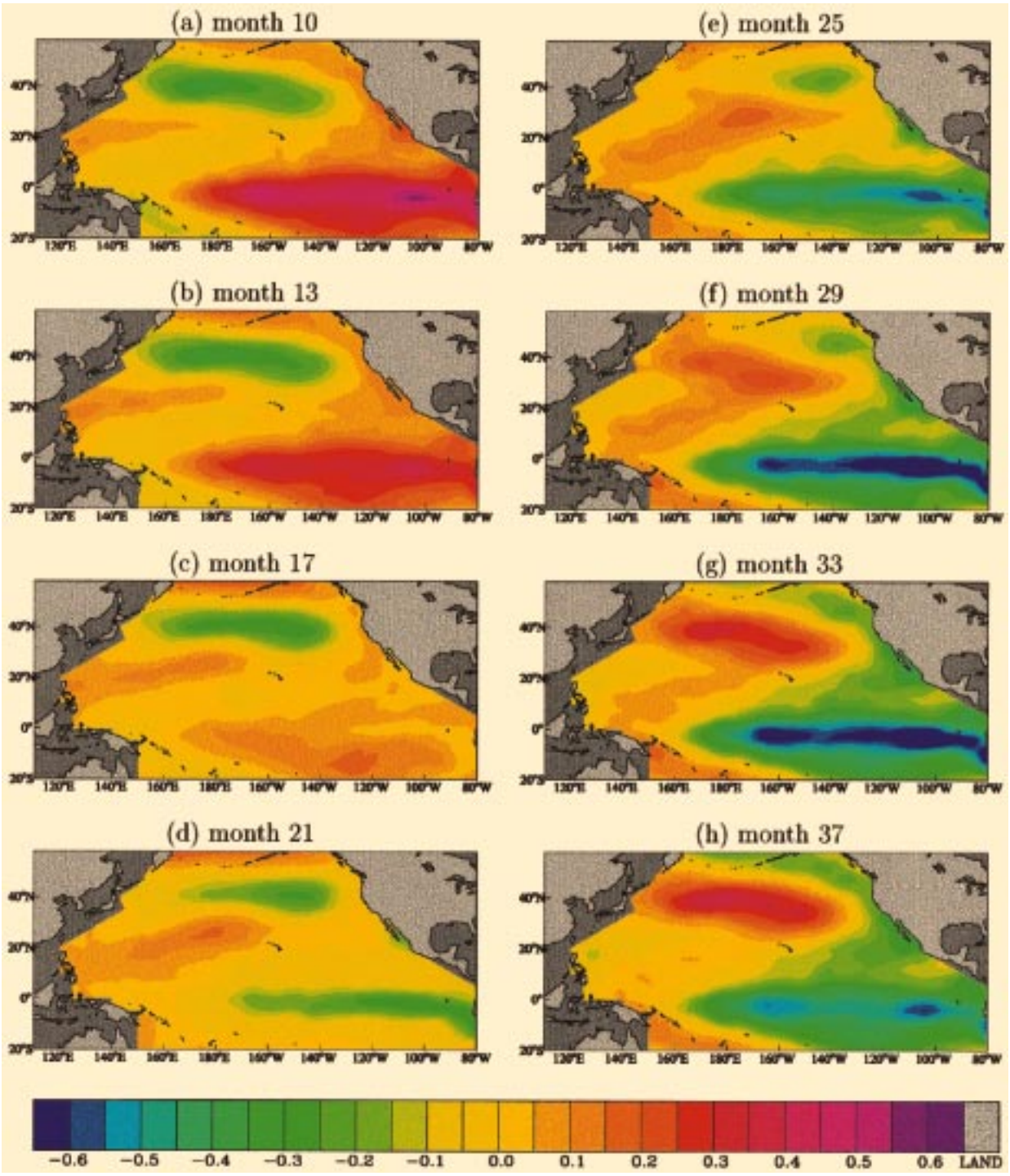

FIG. 5. Spatio-temporal structures of the 51-month oscillation of Pacific SST, represented by the eigenvector sequence ST-EOF2 derived from MSSA with a window length of 61 months. Unit is °C.

ies from 0.60° to 0.68°C (−0.34° to −0.6°C). Negative centers are located in the Gulf of Alaska, the California coast, and in the vicinity of the date line in the Tropics. A positive center appears at the center of the North Pacific. The spatial distribution of SST anomalies is very similar to the slow mode of Zhang et al. (1997): a broader tropical temperature tongue and strong extratropical amplitude. The variance contribution of this mode is 11.4%, which is larger than the contribution to the variance made by the QB mode (ST-PCs 6–7). The

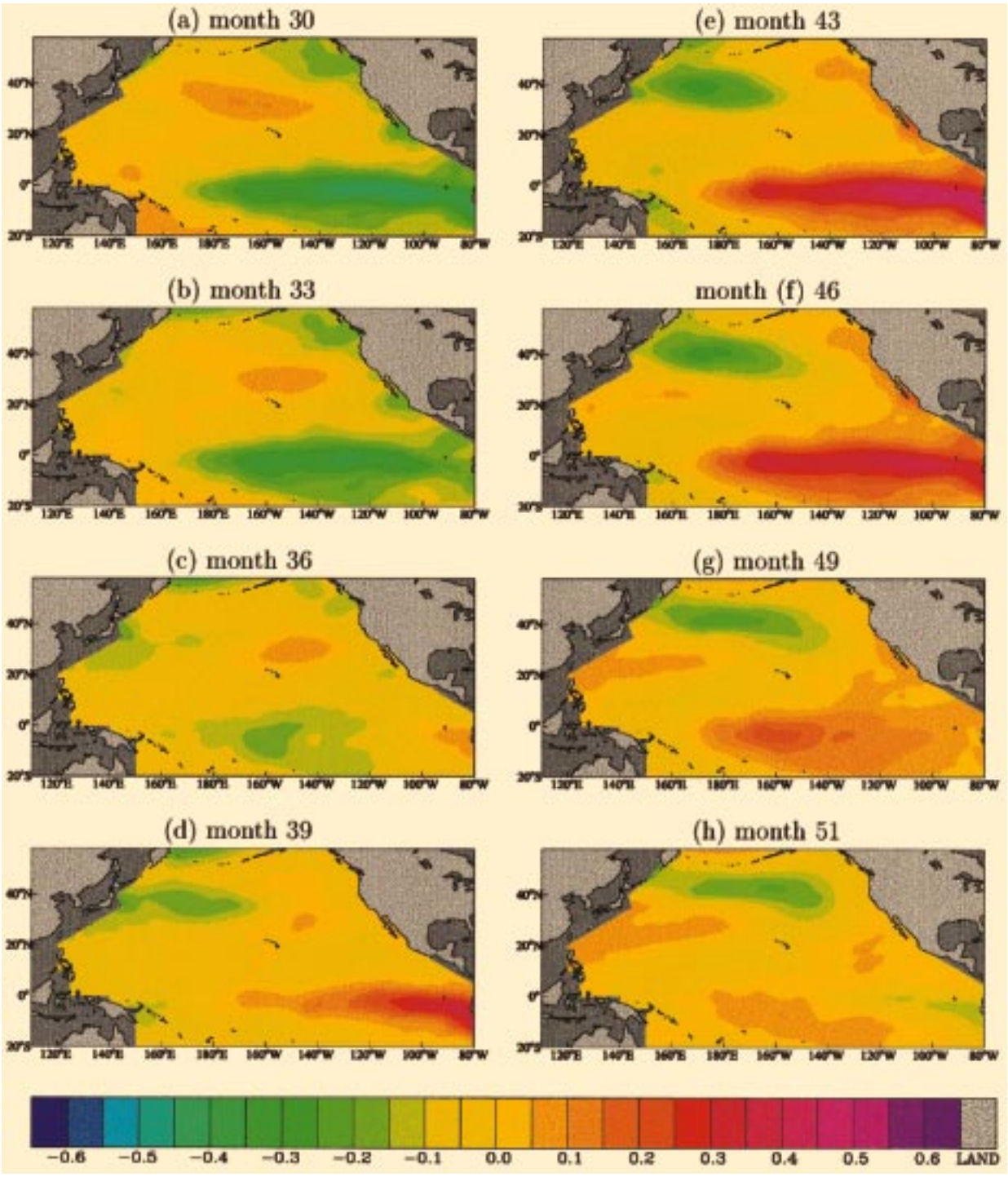

FIG. 6. Same as in Fig. 5 but for the 26-month oscillation, represented by the eigenvector sequence ST-EOF6.

power spectra of ST-PC1 are higher at lower frequencies and there is no peak in the spectra, suggesting that this mode represents a signal with a longer period than can be resolved with the current window length (5 yr). Henceforth this mode is referred to as interdecadal mode and denoted as DE. It should be mentioned that only after removal of QQ and QB from the SST data can the interdecadal mode be significantly different from red noise and that the interdecadal mode explains one-third of variance explained by ENSO modes. These imply that, basinwide, the interdecadal mode is only of secondary importance when compared with ENSO.

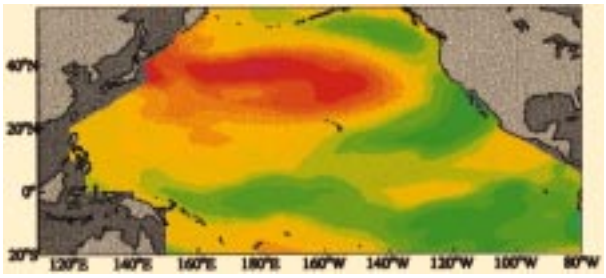

FIG. 7. Spatial structure of ST-EOF1 (°C) averaged from lags 0 to 60 months. The color scale is the same as in Fig. 5.

c. *Distinctions between interdecadal and interannual modes*

The spatio-temporal structure associated with the interdecadal mode is different from those associated with interannual modes, though in certain phases they may have similar spatial distributions as that of SSTA, for example, the mature phase of El Niño or La Niña. First of all, these modes have different dominant frequencies. Second, the characteristic propagation of SSTA shown in the QQ and QB modes does not appear in the interdecadal mode. Third, the interdecadal mode explains more variance in the North Pacific than in the Tropics, whereas the interannual modes contribute more to the total variance in the Tropics. The latter can be clearly seen from the distribution of the SSTA: the interdecadal mode has higher amplitudes in the North Pacific than in the Tropics, whereas the interannual modes display larger absolute values of the anomalies in the Tropics.

The interdecadal and the interannual modes may be of different geographical and possibly different physical origins. Although ENSO has its influence on the global climate, the interannual modes that characterize ENSO are predominantly equatorial Pacific phenomena. To provide a clearer view of relative importance of both interdecadal and interannual modes to the SSTA in different regions of the Pacific, MSSA was performed on the SSTA in the North Pacific and in the tropical Pacific separately (North Pacific: north of 20°N; tropical Pacific: 10°N–10°S). PCA was first performed on the SSTA in the two regions separately: first 10 PCs from each dataset were retained, MSSA was then applied to these PCs with a window length of 61 months.

In the tropical Pacific, two oscillatory ST-PC pairs, ST-PCs 1–2 and 5–6, are identified to be significant with periods of 48 and 26 months, respectively; ST-PC3 is an interdecadal mode that is significantly different from what one may obtain from red noise after removal of ST-PCs 1–2 and 5–6. The evolutions of maps for tropical, interdecadal QQ and QB modes resemble their counterparts in the Pacific SST over the tropical area, respectively. Some phases of tropical QQ (ST-EOF1) and QB (ST-EOF6) are shown in Figs. 8 and 9.

In the North Pacific, the interdecadal mode stands out as the leading ST-EOF, and only one oscillatory pair, ST-PCs 3–4, was identified. The oscillatory pair has a period of about 60 months. The propagation of SSTA of this pair (Fig. 10) is qualitatively similar to those shown for the Pacific QQ mode (Fig. 5), though the period is slightly longer. This oscillation is referred to

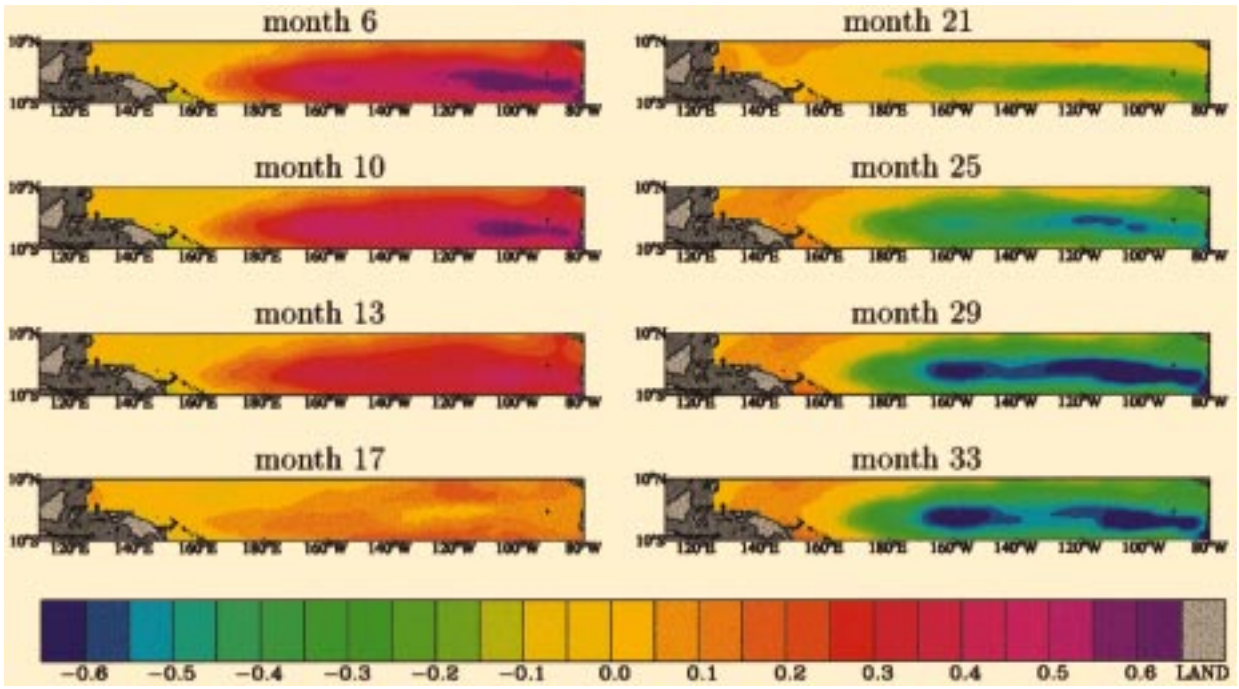

FIG. 8. Same as in Fig. 5 but for the 48-month oscillation of tropical Pacific SST, represented by the eigenvector-sequence ST-EOF1.

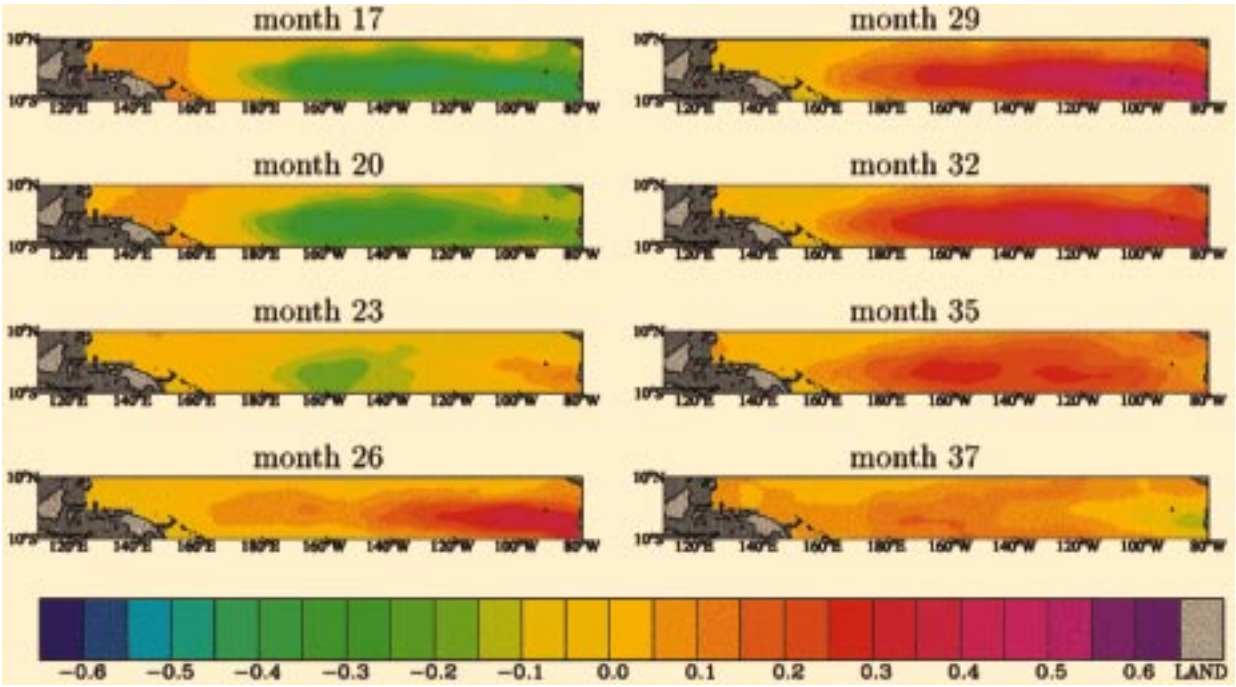

FIG. 9. Same as in Fig. 8 but for the 26-month oscillation, represented by the eigenvector sequence ST-EOF5.

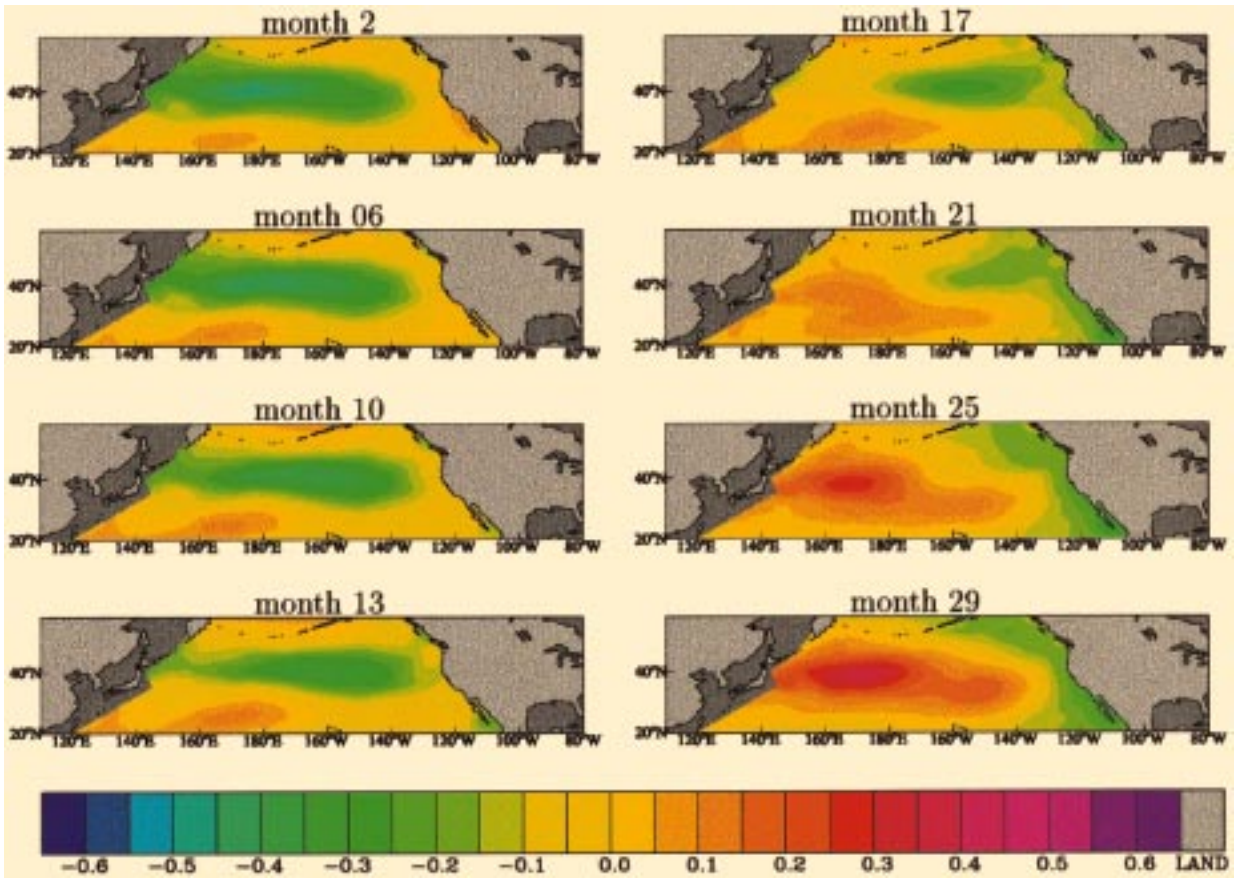

FIG. 10. Same as Fig. 5 but for the 61-month oscillation of North Pacific SST, represented by the eigenvector sequence ST-EOF4.

TABLE 2. Maximum lagged correlations (cor) between ST-PCs obtained by performing MSSA on the SST anomalies in the North Pacific (NP: 58°–20°N), tropical Pacific (TP: 10°N–10°S), and the Pacific basin (PAC: north of 20°S).

Modes	PAC	TP	cor	PAC	NP	cor	TP	NP	cor
DE	1	3	0.895	1	1	0.912	3	1	0.758
QQ	2	1	0.966	2	4	0.695	1	4	0.622
	3	2	0.963	3	3	0.720	2	3	0.552
QB	6	5	0.886						
	7	6	0.832						

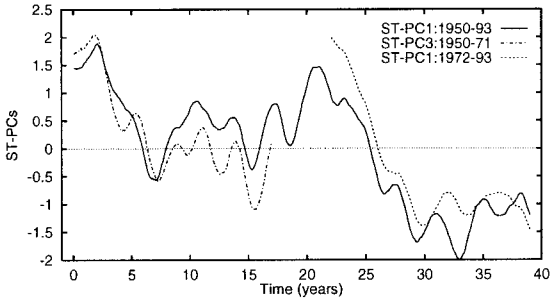

FIG. 11. Time series of Pacific ST-PC1 obtained from data for 1950–93 (solid line), ST-PC3 from data for 1950–71 (dot–dashed line), and ST-PC1 from data for 1972–93 (dashed line). The ST-PC1 of 1950–93 was normalized, ST-PC3 of 1950–71 and ST-PC1 of 1972–93 were scaled by the standard deviation of ST-PC1 of 1950–93 data.

as the North Pacific QQ mode. Both the QQ and the interdecadal mode are significantly different from what one may obtain from red noise. The interdecadal mode explains the same amount of variance as the QQ mode does, implying that this mode is at least as important as the QQ mode in the North Pacific.

To assess the similarity of modes identified in the Pacific and its two subregions, the tropical and North Pacific, the lagged correlations between leading ST-PCs from different areas are computed. Table 2 provides the maximum lagged correlations. The ST-PCs corresponding to interdecadal modes identified in the Pacific, North Pacific, and tropical Pacific (ST-PC1 of both Pacific and North Pacific, ST-PC3 of the Tropics) are highly correlated among each other, indicating that the interdecadal mode is a basinwide phenomena. Table 2 also shows that the oscillatory pairs of ST-PCs relative to QQ found in Pacific, North Pacific and tropical Pacific (ST-PCs 2–3 of Pacific, ST-PCs 1–2 of tropical Pacific, ST-PCs 3–4 of North Pacific) are highly correlated, and that Pacific QQ and tropical QQ are almost identical. These correlations suggest that the QQ identified in the Pacific is mainly contributed by the QQ of the Tropics and that the 60-month oscillation identified in the North Pacific is most likely the response of extratropical SST to the tropical QQ. Lau and Nath (1994) performed numerical experiments of a general circulation model forced by SST in three domains: near-global, tropical Pacific, and mid-latitude North Pacific, and speculated that the extratropical SST may be perturbed by the tropical SST anomalies through the ''atmospheric bridge.'' Our results support their notion that the extratropical SST anomalies are mostly responsive to the tropical oscillation. The ST-PCs representing Pacific and tropical QB (ST-PCs 6–7 of Pacific and ST-PCs 5–6 of tropical Pacific) are also highly correlated. No ST-PC with similar (close) frequency was found in the North Pacific, leading to the conclusion that the QB is mainly a tropical mode.

To summarize, the interdecadal mode, which is associated with the warming in the central equatorial Pacific and the cooling in the central North Pacific after 1976–77, is a basinwide phenomenon. The QQ mode is the strongest in the Tropics and it may have strong extratropical influences—that is, a northeastward propagation of SST anomalies in the extratropics with a period of about 60 months. The QB mode, on the other hand, is localized in the Tropics and has no clear counterpart in the extratropics. Plausible physical explanations for the differences between the interdecadal and the ENSO-related modes can be found in some modeling studies. Miller et al. (1994) and Graham (1994) indicate that decadal-scale changes, such as those associated with the 1976–77 warming, involve links in the coupled atmospheric–oceanic system that are quite different from those associated with ENSO activity: dynamic processes alone can qualitatively reproduce observed SST changes in the central equatorial ocean; however, surface fluxes of heat and radiation played an important role in producing SST changes in other regions.

4. Temporal structure of interdecadal and interannual variability

The temporal structure of interdecadal and interannual modes of variability is discussed in this section. The ST-PC1 time series is plotted in Fig. 11. As shown in Fig. 7, the EOF weights associated with this ST-PC are negative over the west coast of North America and tropical Pacific and are positive over the central North Pacific. Their absolute values are larger in the central North Pacific than elsewhere. The sharp decrease in ST-PC1 implies a decrease in SST over the central Pacific and an increase in SST over other areas. Because of the structure of the EOF, the amplitude of the decrease in the central North Pacific is larger than the increase of SST over the remaining region. The ST-PCs time series corresponding to the 51-month and 26-month oscillations are plotted in Fig. 12. The quasi-quadrennial and quasi-biennial oscillations are clearly shown in the figure.

To show the actual contributions of interdecadal and interannual modes to the variability of SST, the signals associated with those modes are reconstructed. Using the reconstruction technique of Plaut and Vautard (1994), signals representing interdecadal variability are reconstructed from ST-PC 1, those associated with the

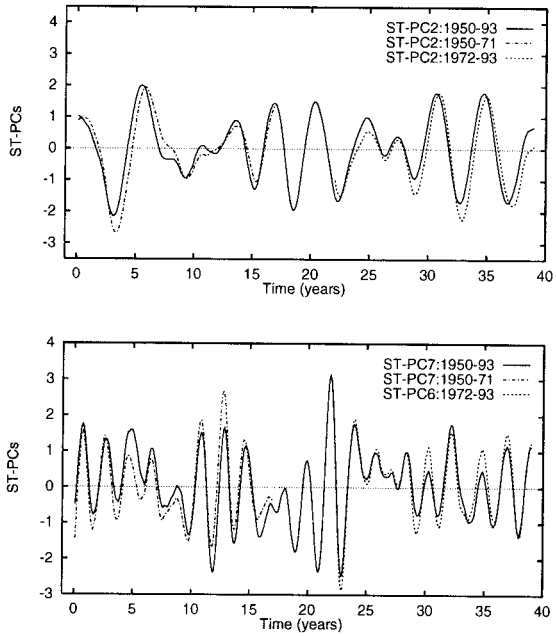

FIG. 12. Time series of ST-PCs for Pacific (top) 51-month and (bottom) 26-month oscillations, obtained from data for 1950–93 (solid lines), from data for 1950–71 (dot–dashed lines), and from data for 1972–93 (dashed lines). ST-PCs of 1950–93 are normalized, while ST-PCs 2 and 6 (or 7) from shorter periods were scaled by the standard deviations of ST-PCs 2 and 7 of 1950–93 data, respectively.

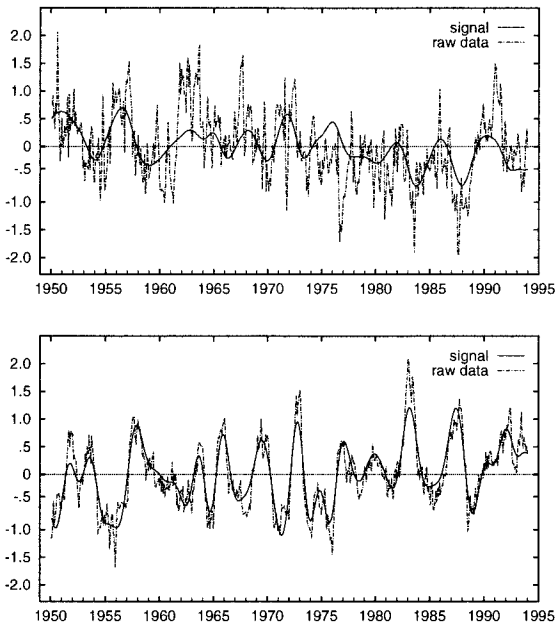

FIG. 13. SST anomalies (in °C) in the North Pacific (top) and tropical Pacific (bottom) from the original time series (dashed lines) and the reconstructed from DE, QQ, and QB time series (solid lines).

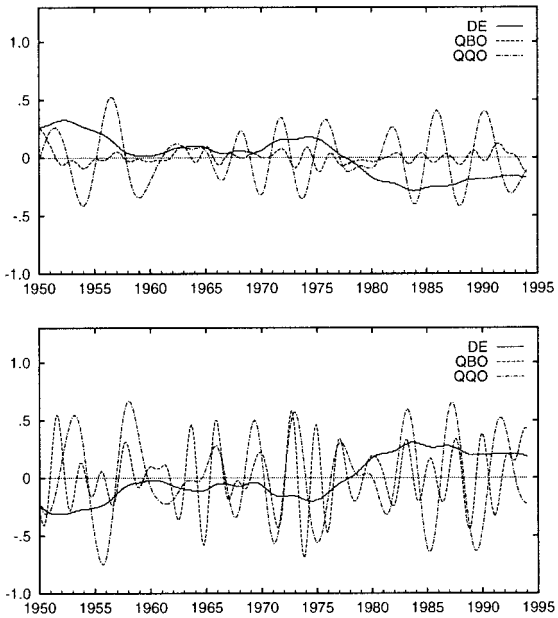

FIG. 14. Reconstructed signal components (in °C) trend, QQ, and QB, in the North Pacific (top) and tropical Pacific (bottom).

QQ from ST-PCs 2–3, and the QB from ST-PCs 6–7. Area averages of SST anomalies contributed by different modes are finally computed for central North Pacific (30°–45°N, 160°E–150°W) and tropical Pacific (4°N–4°S, 160°E–100°W), respectively, and displayed in Fig. 13. The time series of interdecadal and interannual modes for the two regions are plotted in Fig. 14.

The correlation between the reconstructed tropical time series and the SST anomalies is 0.91, indicating a very strong contribution of the combined interdecadal and interannual variability to the ENSO phenomenon. All El Niño and La Niña events are well represented by the reconstruction. Most El Niño episodes during the period coincide with the ''warm'' phase of both QQ and QB, as reported by Jiang et al. (1995). There are also ENSO episodes that result from one mode alone, such as in 1963. Interdecadal mode may be considered as providing a background state for the QQ and QB modes. This background SST increased about 0.4°C from the 1960s to 1980s in the Tropics. More El Niño and fewer La Niña events in recent decades are the manifestation of the superimposition of QQ and QB on a higher background SST in the Tropics. If the interdecadal mode were removed from the tropical SST, the amplitude of El Niño during 1982–83 would have been smaller than that during 1972–73. The correlation between the signal component and the raw SST anomalies over the North Pacific is 0.58. The weaker correlation implies that the contribution of the signal components to the SST variability over this region is much less than those for the Tropics. It is noted that the downward trend of the SST over the North Pacific is well represented by the reconstructed time series (Fig. 13).

5. Conclusions

In this paper, MSSA has been applied to the Pacific SST. Results indicate that a considerable portion of the low-frequency variability of the Pacific SST can be attributed to an interdecadal mode, and quasi-quadrennial and quasi-biennial oscillations. It was found that the interdecadal mode explains larger variance over the North Pacific than over the Tropics, and that the contribution to the total variance by interannual modes (QQ and QB) are largest over the Tropics. The interdecadal mode, which is associated with the warming in the central equatorial Pacific and cooling in the central North Pacific after 1976–77, is a basinwide phenomenon, though the signal is relatively weak in the Tropics. The QQ mode is most pronounced in the Tropics and may have a strong extratropical component consisting of a northeast propagation of SST anomalies in the extratropics with a period of about 60 months. The QB mode, characterized by the westward propagation of SST anomalies in the Tropics is more localized in the Tropics. These findings were further confirmed by applying MSSA on separate SST anomalies in the North Pacific (58°–20°N) and tropical Pacific (10°N–10°S).

As reported in Jiang et al. (1995), in which MSSA was performed on detrended SST anomalies over the tropical Pacific, the QQ and QB modes are the most important modes of ENSO. Reconstructed time series are similar to those of Jiang et al. (1995). Clearly, MSSA is successful in separating low-frequency variability of Pacific SST at different frequency bands. Reconstructed time series combined by adding both the interdecadal and the interannual modes together represent a good fit to the original SST anomalies, particularly in the Tropics. Acting as a background for the interannual modes, the interdecadal mode plays an important role in configuring the state of tropical SST anomalies, which in turn affects the manifestations of ENSO events.

The advantage of using MSSA over the traditional PCA in identifying spatio-temporal structures of climate variability is obvious. Based on the SST data for the period 1900–93, Zhang et al. (1997) separated the time variability of the leading EOFs of the global SST field into two components: one with the ''ENSO cycle-related'' variability on the interannual timescale, and the other a linearly independent ''residual'' mainly comprising all the decade-to-century-scale variability. They found that the two components exhibit remarkably similar spatial signatures in the global SST, and that SST signature in the decade-to-century variability is less equatorially confined in the eastern Pacific and it exhibits larger amplitude over the extratropical North Pacific. Our results not only confirm these findings, but also suggest that the similarity in spatial structure between the two components of Zhang et al. (1997) is due to the similarity between some phases in the ST-EOFs of interdecadal and interannual modes. Indeed, there is mounting evidence (e.g., Jiang et al. 1995; Allen and Smith 1996) suggesting that QQ and QB are two distinctive ENSO modes, though there may be similarity between certain phases of these two oscillations. The interdecadal mode associated with the cooling over the North Pacific and warming over the Tropics since the late 1970s does resemble some phases of interannual modes; however, it has rather different spatio-temporal structures; specifically, it does not propagate SST anomalies (within a 5-yr window) while QQ and QB do.

Acknowledgments. The authors are very much indebted to F. W. Zwiers for reading the first draft of the manuscript and offering a number of valuable comments and suggestions. We also wish to thank W. D. Hogg, A. J. Miller, and an anonymous reviewer for their constructive comments.

REFERENCES

Alexander, M. A., 1990: Simulation of the response of the North Pacific Ocean to the anomalous atmospheric circulation associated with El Niño. *Climate Dyn.,* **5,** 53–65.

Allen, M. R., and L. A. Smith, 1996: Monte Carlo SSA: Detecting irregular oscillations in the presence of colored noise. *J. Climate,* **9,** 3373–3404.

Barrodale, I., and R. E. Erickson, 1980: Algorithms for least-squares linear prediction and maximum entropy spectral analysis. Part I: Theory. *Geophysics,* **45,** 420–432.

Deser, C., and M. L. Blackmon, 1995: On the relationship between tropical and North Pacific sea surface temperature variations. *J. Climate,* **8,** 1677–1680.

Graham, N. E., 1994: Decadal-scale climate variability in the tropical and North Pacific during the 1970s and 1980s: Observations and model results. *Climate Dyn.,* **10,** 135–162.

Jiang, N., J. D. Neelin, and M. Ghil, 1995: Quasi-quadrennial and quasi-biennial variability in the equatorial Pacific. *Climate Dyn.,* **12,** 101–112.

Lau, N.-C., 1997: Interactions between global SST anomalies and the midlatitude atmospheric circulation. *Bull. Amer. Meteor. Soc.,* **78,** 21–33.

——, and M. J. Nath, 1994: A modeling study of the relative roles of tropical and extratropical SST anomalies in the variability of the global atmosphere–ocean system. *J. Climate,* **7,** 1184–1207.

Miller, A. J., D. R. Cayan, T. P. Barnett, N. E. Graham, and J. M. Oberhuber, 1994: Interdecadal variability of the Pacific Ocean: Model response to observed heat flux and wind stress anomalies. *Climate Dyn.,* **9,** 287–302.

North, G. R., T. L. Bell, R. F. Cahalan, and F. J. Moeng, 1982: Sampling errors in the estimation of empirical orthogonal functions. *Mon. Wea. Rev.,* **110,** 699–706.

Plaut, G., and R. Vautard, 1994: Spells of low-frequency oscillations and weather regimes in the Northern Hemisphere. *J. Atmos. Sci.,* **51,** 210–236.

Reynolds, R. W., and E. M. Rasmusson, 1983: The North Pacific sea surface temperature associated with El Niño. *Proc. Seventh Annual Climate Diagnostic Workshop,* Boulder, CO, NOAA, 298–310.

Tanimoto, Y., N. Iwasaka, K. Hanawa, and Y. Toba, 1993: Characteristic variations of sea surface temperature with multiple time scales in the North Pacific. *J. Climate,* **6,** 1153–1160.

Trenberth, K. E., 1990: Recent observed interdecadal climate changes in the Northern Hemisphere. *Bull. Amer. Meteor. Soc.,* **71,** 988–993.

——, and J. W. Hurrell, 1994: Decadal atmosphere–ocean variations in the Pacific. *Climate Dyn.,* **9,** 303–319.

——, and T. J. Hoar, 1996: The 1990–1995 El Niño–Southern Oscillation event: Longest on record. *Geophys. Res. Lett.,* **23,** 57–60.

Vautard, R., P. Yiou, and M. Ghil, 1992: Singular spectrum analysis: A toolkit for short, noisy chaotic signals. *Physica D,* **58,** 95–126.

Wallace, J. M., C. Smith, and C. S. Bretherton, 1992: Singular value decomposition of wintertime sea surface temperature and 500-mb height anomalies. *J. Climate,* **5,** 561–576.

Wang, B., 1995: Interdecadal changes in El Niño onset in the last four decades. *J. Climate,* **8,** 267–285.

Wang, X., J. Corte-Real, and X. Zhang, 1996: Low-frequency oscillations and associated wave motions over Eurasia. *Tellus,* **48A,** 238–253.

Woodruff, S. D., R. J. Slutz, R. L. Jenne, and P. M. Steurer, 1987: A comprehensive ocean–atmosphere data set. *Bull. Amer. Meteor. Soc.,* **68,** 1239–1250.

Zhang, Y., J. M. Wallace, and D. S. Battisti, 1997: ENSO-like interdecadal variability: 1900–93. *J. Climate,* **10,** 1004–1020.